Springer Link

Richard B. Hetnarski
Encyclopedia of Thermal Stresses
10.1007/978-94-007-2739-7_808

Shaped Metal Deposition Processes

Carlos Agelet de Saracibar [1,2], Andreas Lundbäck [3], Michele Chiumenti [1,2] and Miguel Cervera [1,2]

(1) ETS Ingenieros de Caminos, Canales y Puertos, Universidad Politécnica de Cataluña, Barcelona Tech, Barcelona, Spain
(2) International Center for Numerical Methods in Engineering (CIMNE), Barcelona, Spain
(3) Department of Engineering Sciences and Mathematics, Mechanics of Solid Materials, Luleå University of Technology, Luleå, Sweden

Carlos Agelet de Saracibar (Corresponding author)
Email: agelet@cimne.upc.edu

Andreas Lundbäck
Email: Andreas.Lundback@ltu.se

Michele Chiumenti
Email: michele@cimne.upc.edu

Miguel Cervera
Email: miguel.cervera@upc.edu

Without Abstract

Overview

The shaped metal deposition (SMD) process is a novel manufacturing technology which is similar to the multi-pass welding used for building features such as lugs and flanges on components [*1*–*7*]. This innovative technique is of great interest due to the possibility of employing standard welding equipment without the need for extensive new investment [*8*, *9*]. The numerical simulation of SMD processes has been one of the research topics of great interest over the last years and requires a fully coupled thermo-mechanical formulation, including phase-change phenomena defined in terms of both latent heat release and shrinkage effects [*1*–*6*]. It is shown how computational welding mechanics models can be used to model SMD for prediction of temperature evolution, transient, as well as residual stresses and distortions due to the successive welding layers deposited. Material behavior is characterized by a thermo-elasto-viscoplastic constitutive model coupled with a metallurgical model [*6*]. Two different materials, nickel superalloy 718 [*6*] and titanium Ti-6Al-4 V

[*7*], are considered in this work. Both heat convection and heat radiation models are introduced to dissipate heat through the boundaries of the component. The in-house-developed coupled thermo-mechanical finite element (FE) software COMET [*10*] is used to deal with the numerical simulation, and an ad hoc activation methodology is formulated to simulate the deposition of the different layers of filler material.

Introduction

The shaped metal deposition (SMD) is a manufacturing technology, originally patented by Rolls-Royce plc, similar to multi-pass welding, which can be used to build components such as flanges or lugs directly on fabricated components. Parts are built layer by layer depositing the melted material along a predefined path. At each pass, a new layer is deposited on the previous substrate allowing the fabrication of the desired geometry. During an SMD process, the solidification occurs rapidly in a small and localized volume, resulting in a fine as deposited microstructure. The filler material is cooled mainly by conduction through the (much cooler) substrate, leading to very high solidification rates. On one hand, this is an advantage over alternative manufacturing processes such as casting, forging, or machining because the quality of the final component presents a much finer grain size as well as the reduction of both the buy-to-fly ratio and the production time. On the other hand, the material is subject to thermal cycles changing the microstructure of the heat-affected zone (HAZ). This temperature evolution may lead to the re-melting of the material and, in any case, it induces a continuous change in the microstructure during the full process. Irregular liquation and cracking in the HAZ is an undesired phenomenon that becomes a drawback of the SMD process. The combination of liquid films along grain boundaries and thermal (tensile) stresses due to the thermal cycles may lead to the formation of irregular cracks.

The high temperature gradients generated by the welding process induce distortions on the fabricated structure, posing difficulties for later assembling processes. Nowadays, the expensive trial-and-error procedures, based on the knowledge and experience coming from previous similar designs, are the standard industrial practice. The numerical simulation of the process is a very interesting alternative to optimize the welding strategy. Both the thermal and the mechanical behavior can be predicted, leading to an optimal manufacturing design for large welded structures.

This entry shows an accurate numerical simulation of the SMD process, providing the temperature evolution, distortion, and stress fields generated during the process. This makes it possible to estimate the hot cracking risk, as well as optimizing the manufacturing design.

To this end, this entry presents a detailed description of the FE technology used to simulate the deposition of the material during the welding process. The modeling shares many features with welding simulations and particularly multi-pass welding. However, there are special issues

concerning the modeling of the filler materials that build up the wanted features. The strategy adopted consists on an element activation procedure, which allows switching on the elements according to the welding path defined by the user. Also of importance is a constitutive model that is able to describe the material behavior in all the temperature range of the process.

Coupled Thermo-Mechanical Model

The local system of partial differential equations governing the coupled thermo-mechanical initial boundary value problem is defined by the linear momentum and energy balance equations, restricted by the inequalities arising from the second law of the thermodynamics. This system must be supplemented by suitable constitutive equations. Additionally, one must supply suitable prescribed boundary and initial conditions.

Thermal Model

The local form of the energy balance equation takes the form

$$\dot{H}(T) = -\nabla \cdot \mathbf{q}(T) + R + \mathfrak{D} \quad \text{in} \quad \Omega \tag{1}$$

where T is the absolute temperature, $H(T)$ is the enthalpy per unit of volume, $\mathbf{q}(T)$ is the heat flux vector per unit of surface, R is an internal heat source rate per unit of volume, $\mathfrak{D}$ is the internal dissipation rate per unit of volume, and ∇ is the Nabla operator.

The enthalpy rate per unit of volume is given by

$$\dot{H}(T) = c(T)\dot{T} + \dot{L}_{pc}(T) \tag{2}$$

where $c(T)$ is the temperature-dependent heat capacity coefficient and $\dot{L}_{pc}(T)$ is the rate of latent heat released during the solidification process given by

$$\dot{L}_{pc}(T) = L_{pc}\dot{f}_l(T) = -L_{pc}\dot{f}_s(T) \tag{3}$$

where L_{pc} is the total amount of latent heat released/absorbed during the phase change, $f_l(T) = 1 - f_s(T)$ is the liquid fraction, and $f_s(T)$ is the solid fraction [*6*].

For the nickel superalloy 718, using Scheil's additivity rule and assuming there is no solid state diffusion during the solidification, the solid fraction is computed in terms of the temperature, fusion and liquidus temperature, nominal alloy composition, and partition coefficient, that is. ratio between the composition of the solid and the composition of the liquid at equilibrium [*6*]. Solid fraction for the titanium Ti-6Al-4V is computed in a similar way, providing the latent heat and the solidus and liquidus temperature [*7*].

The heat flux per unit of surface $\mathbf{q}(T)$ is given by Fourier's law:

$$\mathbf{q}(T) = -k(T)\nabla T \tag{4}$$

where $k(T)$ is the temperature-dependent thermal conductivity parameter.

The internal heat source rate per unit of volume plays a key role in the numerical simulation of SMD processes, and different models have been proposed in the literature. Here, the internal heat source rate per unit of volume is given by [*6*]

$$R = \eta \frac{VI}{V_{feed}} \tag{5}$$

where *V* is the arc voltage, *I* is the welding current, V_{feed} is the volume of the filler material melted by the feeding system during the current time step, and η is the welding efficiency parameter. Thus, we assume constant heat distribution over the filler material. Use of heat source models with, for example, a Gaussian distribution will require a much finer finite element mesh than presently possible to use for large 3D models of SMD.

For the numerical simulation of SMD processes, the thermo-mechanical dissipation rate per unit of volume can be neglected in comparison with the large heat inputs from the weld source. Heat loss by radiation, important at high temperatures in the HAZ, is computed using the Stefan-Boltzmann. This effect can be accounted for by modifying the efficiency parameter of the heat source without a significant loss of accuracy in the simulation. Heat dissipated by convection can be computed using Newton's law [*6*].

Mechanical Model

The local form of the linear momentum balance equation, assuming quasi-static conditions, takes the form

$$\nabla \cdot \sigma(\mathbf{u}, T) + \mathbf{f} = \mathbf{0} \quad \text{in} \quad \bar{\Omega} \tag{6}$$

where $\sigma(\mathbf{u}, T)$ is the Cauchy stress tensor, $\mathbf{u}$ is the vector of displacements, and $\mathbf{f}$ is the vector of body forces per unit of volume. The Cauchy stress tensor can conveniently be split into

$$\sigma(\mathbf{u}, T, p) = \mathbf{s}(u, T) + p\mathbf{1} \tag{7}$$

where $\mathbf{s}(\mathbf{u}, T)$ is the deviatoric part of the Cauchy stress tensor, *p* is the pressure, viewed as an independent variable, and $\mathbf{1}$ is the second-order unit tensor. This is practical in case of deviatoric plasticity where the pressure is a pure thermo-elastic update. However, this split is necessary if a mixed displacement-pressure finite element is used [*6*, *11–13*]. This approach was used for the alloy 718 SMD case. A corresponding displacement formulation with underintegration of the volumetric strain was used for the Ti6-4 SMD case. Both approaches remove the risk for locking due to the plastic incompressibility condition [*6*, *11–13*]. The governing equations for the mechanical problem, given by the local mixed form of the linear momentum balance equation and the pressure constitutive equation, take the form

$$\left.\begin{array}{c} \nabla \cdot \mathbf{s}(\mathbf{u},\mathbf{T}) + \nabla p + \mathbf{f} = \mathbf{0} \\ \nabla \cdot \mathbf{u} - e_T(T) - \dfrac{f_s(T)}{K(T)}\, p = 0 \end{array}\right\} \quad \text{in} \quad \bar{\Omega} \tag{8}$$

where $K(T)$ is the temperature-dependent bulk modulus and $e_T(T)$ is the volumetric thermal deformation which takes into account the thermal shrinkage during the phase change, from the liquidus temperature T_l to the solidus temperature T_s, and the thermal contraction during the cooling process, from solidus temperature to room temperature, and is defined as

$$e_T(T) = \begin{cases} \dfrac{\rho(T_s) - \rho(T_l)}{\rho(T_s)} + 3\big[\alpha(T)\big(T - T_{ref}\big) \\ -\alpha(T_0)\big(T_0 - T_{ref}\big)\big] \quad \text{if} \quad T \le T_s \\ 0 \quad \text{if} \quad T_l \le T \\ \dfrac{\rho(T) - \rho(T_l)}{\rho(T_s)} \quad \text{if} \quad T_s \le T \le T_l \end{cases} \tag{9}$$

where $\rho(T)$ is the temperature-dependent mass density, $\alpha(T)$ is the temperature-dependent secant thermal expansion coefficient, see entry Welding Stresses, T_0 is the initial temperature, the temperature at which no thermal strains exist, and T_{ref} is the reference temperature, the temperature used for a secant-based definition of the thermal expansion coefficient.

The deviatoric part of the constitutive equation for alloy 718 is given by

$$\mathbf{s}(\mathbf{u},T) = 2\,\frac{G(T)}{f_s(T)}\,\mathrm{dev}\Big(\widehat{\nabla}\mathbf{u} - \mathbf{e}^{\mathrm{p}}(\mathbf{u},\mathbf{T})\Big) \tag{10}$$

where $G(T)$ is the temperature-dependent shear modulus, $\mathrm{dev}(\cdot)$ denotes the deviatoric operator, $\widehat{\nabla}(\cdot)$ denotes the symmetric gradient operator, and $\mathbf{e}^{p}(\mathbf{u},\mathbf{T})$ is the plastic strain. Here, an associative rate-dependent J2 thermo-plastic model with isotropic hardening is considered, and the yield function is given by [*6*]

$$\phi(\mathbf{s},q,T) = \|\mathbf{s}\| - R_{VM}(q,T) \tag{11}$$

where q is the isotropic hardening parameter in the stress space and $R_{VM}(q,T)$ is the temperature-dependent radius of the von Mises yield surface given by

$$R_{VM}(q,T) = f_s\,(T)\sqrt{\frac{2}{3}}\,(\sigma_0(T) - q) \tag{12}$$

where $\sigma_0(T)$ is the temperature-dependent initial yield stress.

Note that for the liquid state, that is, $T \ge T_l$, the solid fraction is zero, the volumetric thermal deformation given by (9) is zero, and the radius of the von Mises yield surface given by (12) goes to zero, yielding an incompressible rate-dependent rigid-plastic behavior characterized by $\nabla \cdot \mathbf{u} = 0$ and a Norton-Hoff law arising from the plastic flow rule [*6*].

Prediction of the hot cracking phenomena is a difficult task from a computational point of view [*14*]. Here, for the nickel superalloy 718, a continuum damage model based on macroscopic quantities is used [*6*, *15*]. The objective of the hot cracking model is to prevent from an excessive (tensile) stress level when the material, still partially liquid, contracts (shrinkage) but all the surrounding phase has solidified. Further details about the damage-enhanced model to predict hot cracking can be found in [*6*].

A physical-based plasticity model, as described in the entry "Constitutive Models, Physically Based Models for Plasticity" is used to describe the plastic behavior of Ti6-4. It accounts for low temperature and high temperature plasticity including stress relaxation due to recovery by glide and climb of dislocations. It also accounts for the phase change that Ti6-4 is subject to during the temperature cycles [*12*].

Finite Element Modeling of the SMD Process

The numerical simulation of an SMD process requires an element activation technology to reproduce the deposition of the melted material along a prescribed path. Here, the so-called born-dead elements technique has been used. This activation strategy classifies the elements defined in the original mesh into active, inactive, and activated elements. The active elements, such as the elements defining the base material, are computed and assembled into the global matrix. The inactive elements, such as the entire discretized domain defining the welding path, have been generated, but they are not assumed as part of the model and do not play any role in the computational model. At each time step, a number of elements, defined as activated elements, are switched on according to the deposition of the filler material. Only active and activated elements are assembled into the solution model. At each time step of the simulation, the profile of the solution matrix, as well as the number of equations, is changing according to the activation process [*6*]. The activation can with advantage be performed independently in the thermal and mechanical solutions as discussed in the entry "Repair Welding and Local Heat Treatment".

It can be noted that the boundary of the computational domain is changing due to the activation process, requiring a specific searching strategy to update the active surface at each time step of the numerical simulation. This is important to be able to correctly apply boundary conditions, such as the heat radiation and heat convection fluxes, according to the activation process [*6*].

SMD processes induce extremely high temperature gradients that can provoke unrealistic temperature overshoots and undershoots in the numerical solution, especially if coarse meshes and large time steps are used. This has been avoided in the alloy 718 SMD case using a nodal (Lobatto) integration rule which stabilizes the solution introducing a small numerical diffusivity into the heat conduction problem [*6*, *13*, *16*]. A lumped heat capacity matrix was used in the Ti6-4 SMD case,

which also results in that any overshoots or undershoots are avoided.

Computational Simulations

The computational model presented in the previous sections for the nickel superalloy 718 has been implemented in CIMNE's in-house-developed coupled thermo-mechanical FE software COMET [*10*]. The Ti6-4 SMD case was solved using MSC.Marc combined with user routines for generating the weld paths, heat input, and the addition of filler material [*7*].

Alloy 718 SMD Process

This 10-layer SMD test case is intended to assess the accuracy of the proposed model when a fully coupled thermo-mechanical analysis is applied to predict the temperature evolution, distortions, and residual stresses of the structure.

The experimental setting is shown in Fig. 1. We consider a rectangular base plate, 275 [mm] long, 100 [mm] wide, and 12 [mm] thick. The SMD process consists of two preheating passes (no feeding material is used) followed by the deposition of 10 layers of material. An isostatic clamping of the base plate is assumed to avoid any stress concentration induced by the thermal deformation of the plate. The material is nickel superalloy 718.

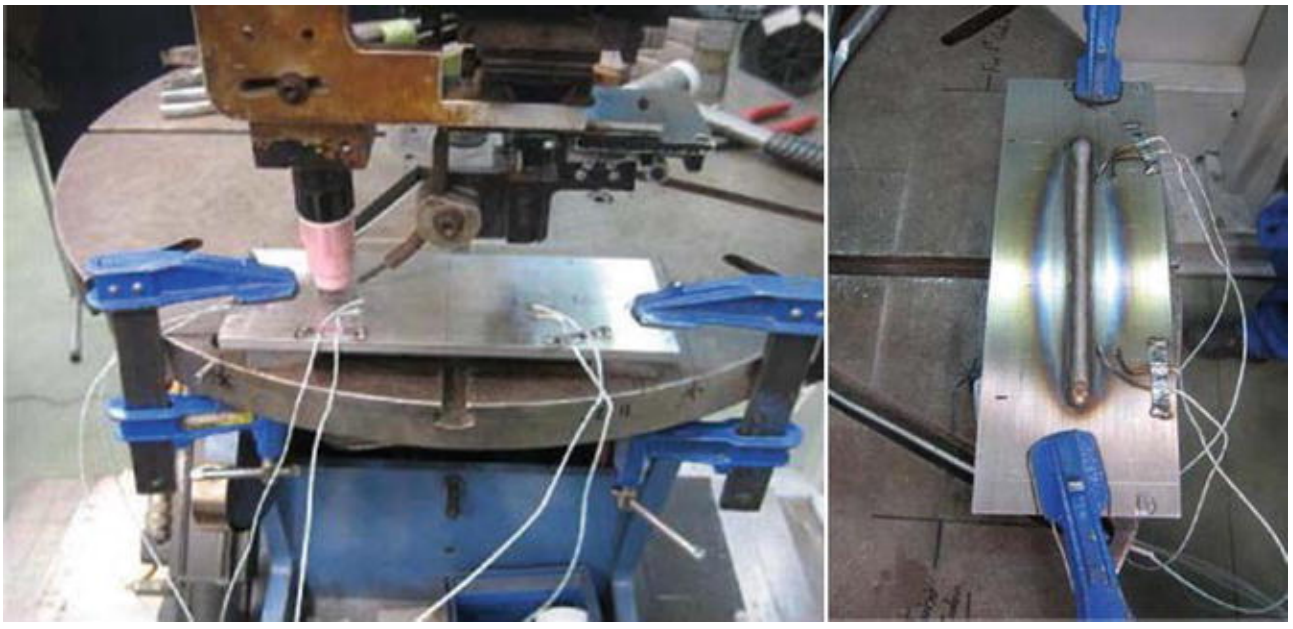

Fig. 1

10-Layer SMD test: experimental setting (*left*) and clamping system (*right*)

The finite element model, shown in Fig. 2, consists of 54.862 Q1/P0 hexahedral elements and 34.012 nodes. Figure 3 compares the temperature evolution at different thermocouple locations.

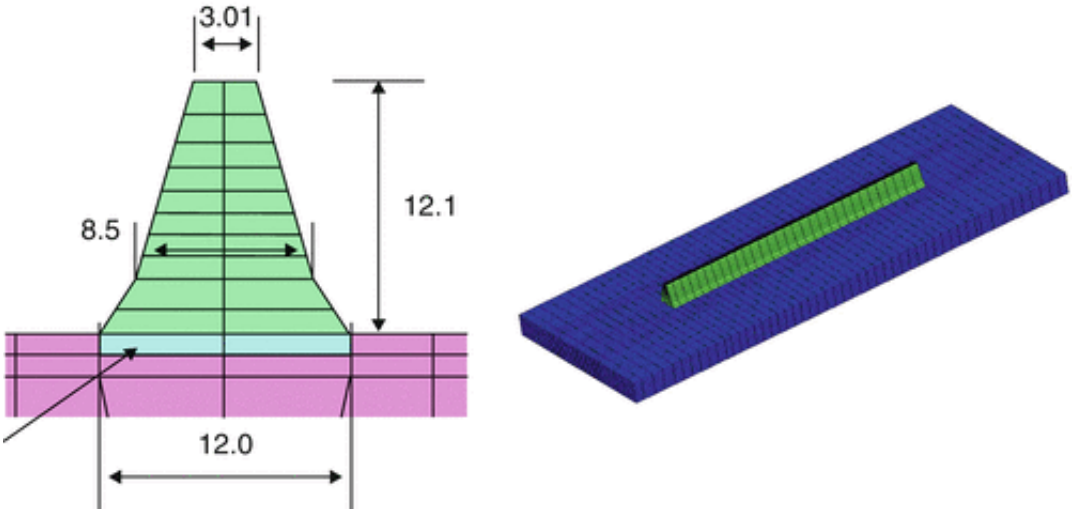

Fig. 2

10-Layer SMD test: cross section (*left*) and FE mesh used for the numerical simulation (*right*)

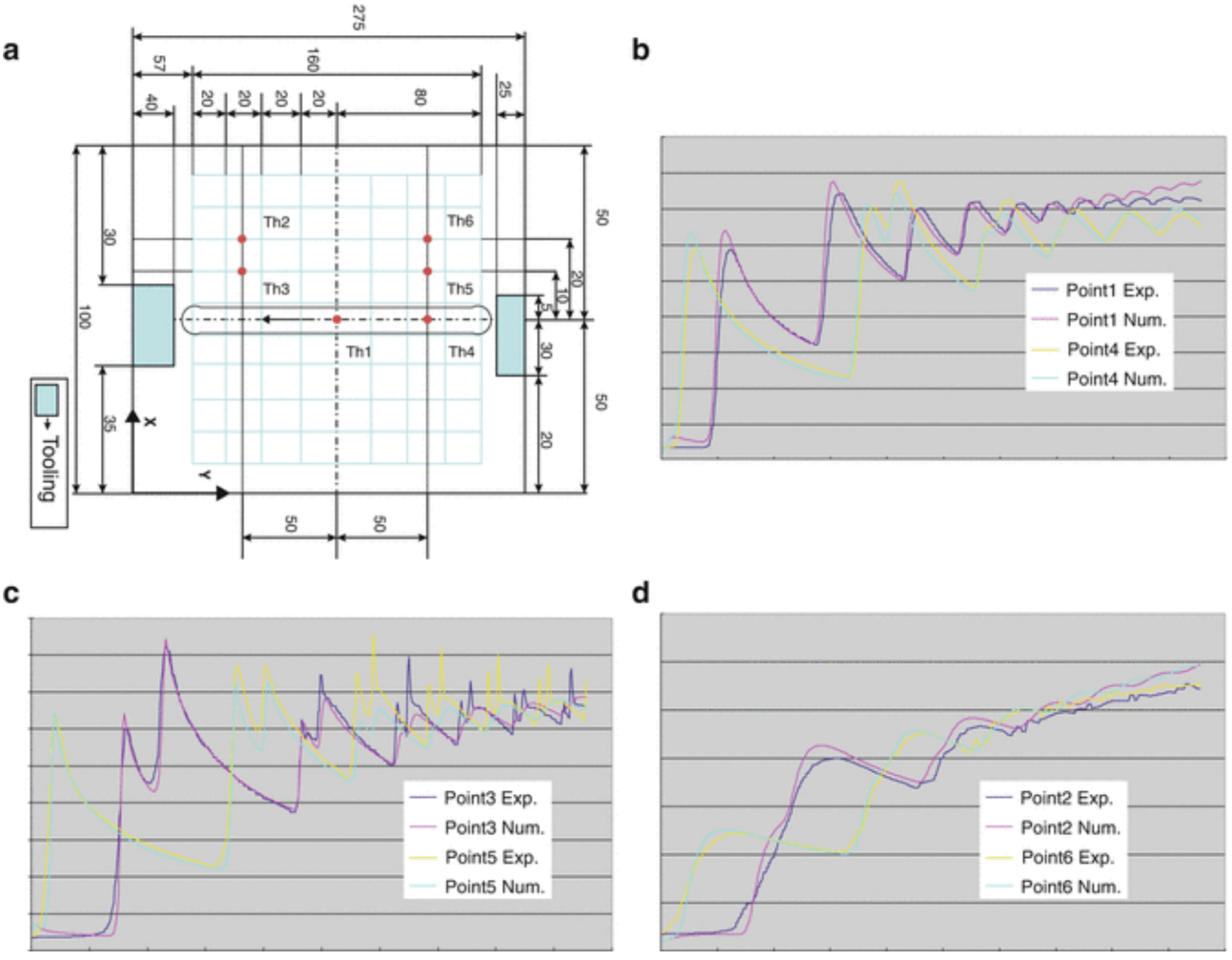

Fig. 3

10-Layer SMD test: thermocouples location (*top left*); comparison between numerical and experimental results for thermocouples 1 and 4 (*top right*), thermocouples 3 and 5 (*bottom left*), and thermocouples 2 and 6 (*bottom right*)

The comparison between experimental and numerical deformation for two transversal and two

longitudinal sections is presented in Figs. 4 and 5, respectively. It is possible to observe how numerical results underestimate the deflection. One possible reason is the kinematic formulation adopted. Most likely, the results would look better using a large-strain formulation but, on the other hand, such a formulation is too expensive from the computational point of view when running industrial cases.

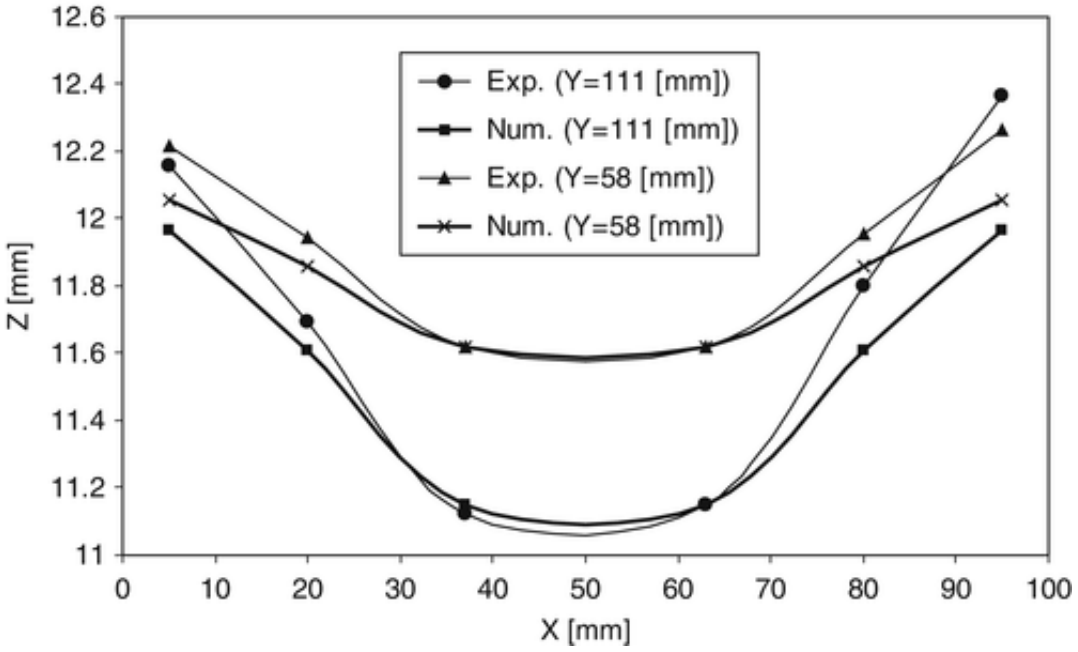

Fig. 4

10-Layer SMD test: comparison between numerical and experimental deformation for two transversal sections. Z-displacement for Y = 111 [mm], Z-displacement for Y = 58 [mm]

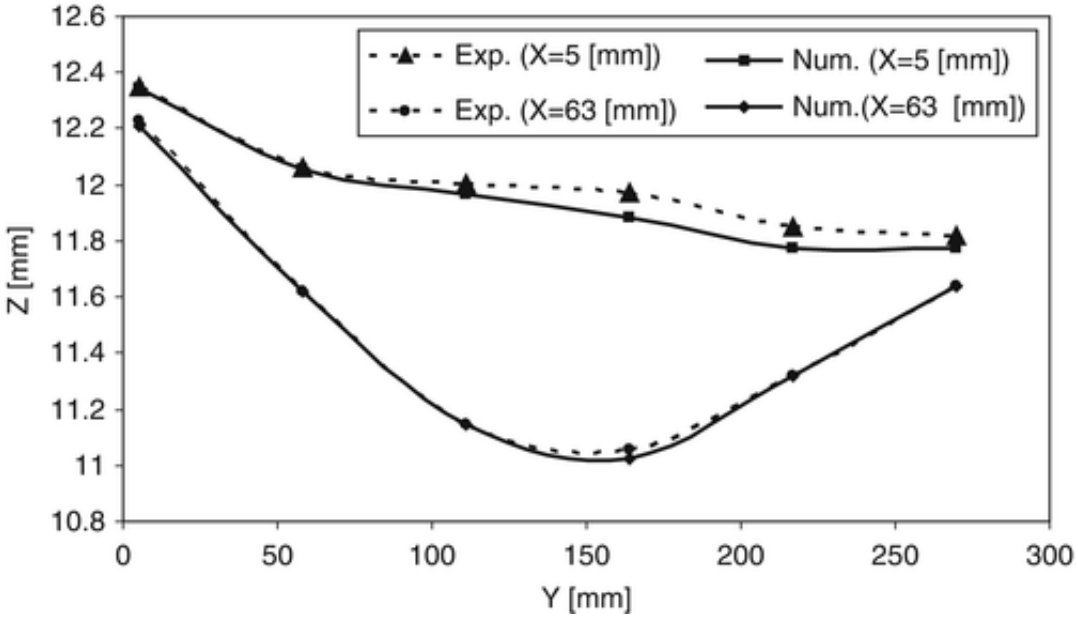

Fig. 5

10-Layer SMD test: comparison between numerical and experimental deformation for two longitudinal sections. Z-displacement for X = 5 [mm], Z-displacement for X = 63 [mm]

Finally, Fig. 6 compares the residual stress field at three different locations of the strain gauges. Hole-drilling method has been used to obtain the residual stresses at the different locations. J2 von Mises stress indicator has been chosen to check the full stress tensor behavior. As average, a 10 % error between the experimental and the numerical results is observed. An overall good accuracy of the numerical model proposed can be observed.

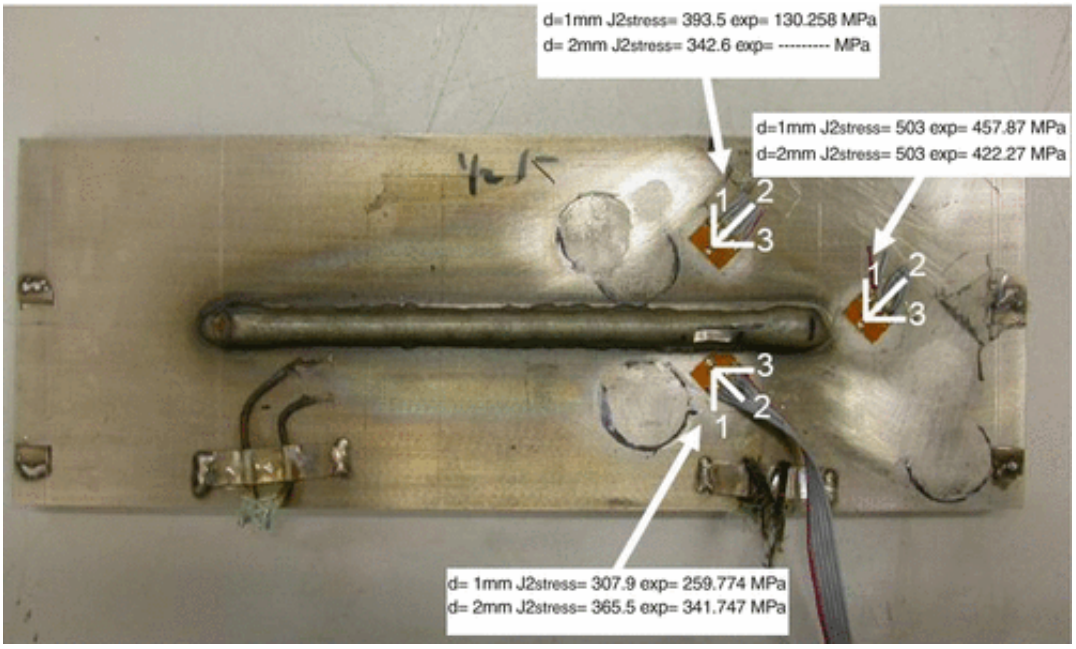

Fig. 6

10-Layer SMD test: comparison between numerical and experimental von Mises stresses at three different strain gauge locations

Ti6-4 SMD Process

Figure 7 shows the experimental setup used for validation of the FE model. It shows the plate with the starting point and weld order for each weld path. In total, 10 layers are added with a total height of 9 mm. The base plate is 200 mm long, 100 mm wide, and 3.2 mm thick. The fixturing system with four pairs of tightening screws on each side of the plate can also be seen in the figure. There are two point supports on the bottom side of the plate, denoted A and B in the figure.

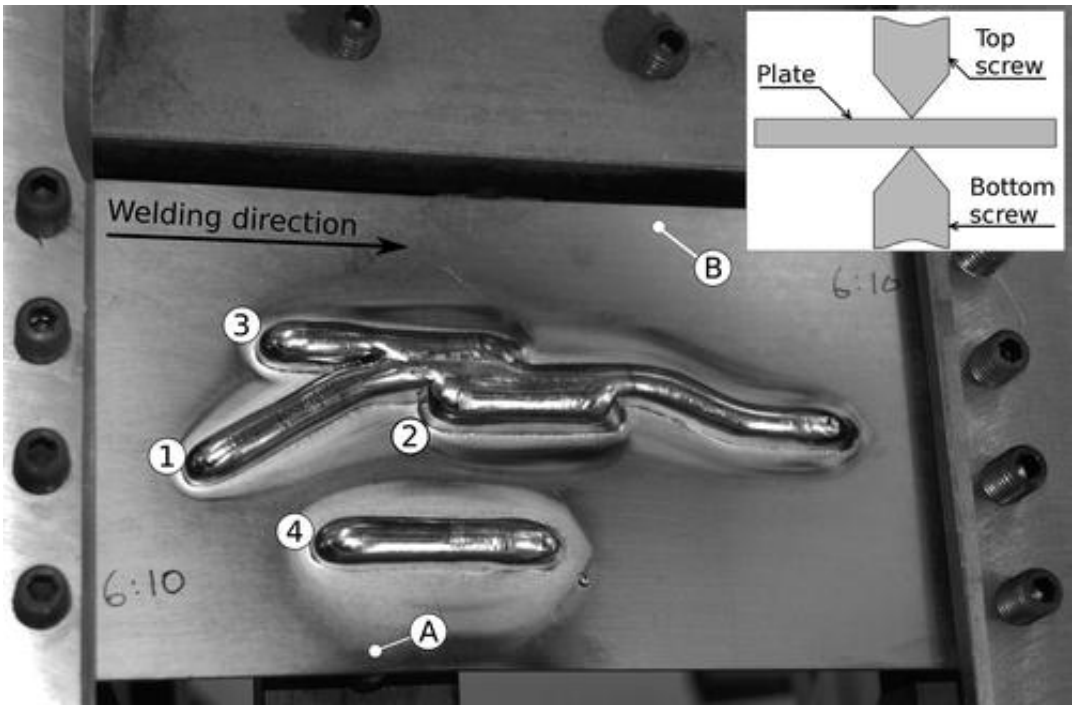

Fig. 7

Experimental setup, plate after finished welding. The plate is still in the fixture

In Fig. 8, the computed thermal field during build up of the seventh layer is shown. The finite element model consists of approximately 13,000 linear hexahedral elements. The note I in Fig. 8 shows the position where the out-of-plane deformation measurement was performed. Note II shows the position of the temperature measurement. The temperature measurement is done with a calibrated pyrometer. The focus point of the pyrometer is positioned 2 mm above the base plate and in the middle of weld pass 4.

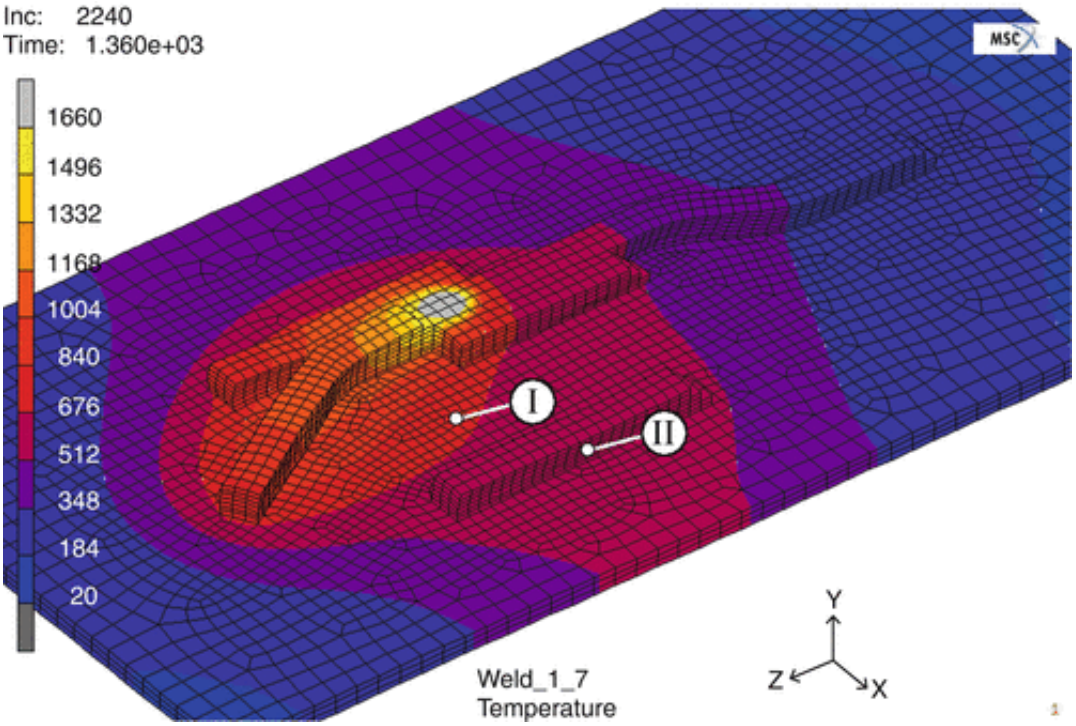

Fig. 8

Computed temperature field during the build up of the seventh layer

The measured and computed temperatures for position II are shown in Fig. 9. A number of peaks can be observed for the measured curves, which are not found in the computed temperature. There are spurious temperature peaks due to reflections from the weld arc while welding the other sequences. Figure 10 shows a comparison of the measured and computed out-of-plane deformations. Here, the overall trend of the deformations is captured very well, but the model overpredicts the changes in deformation for each welding cycle.

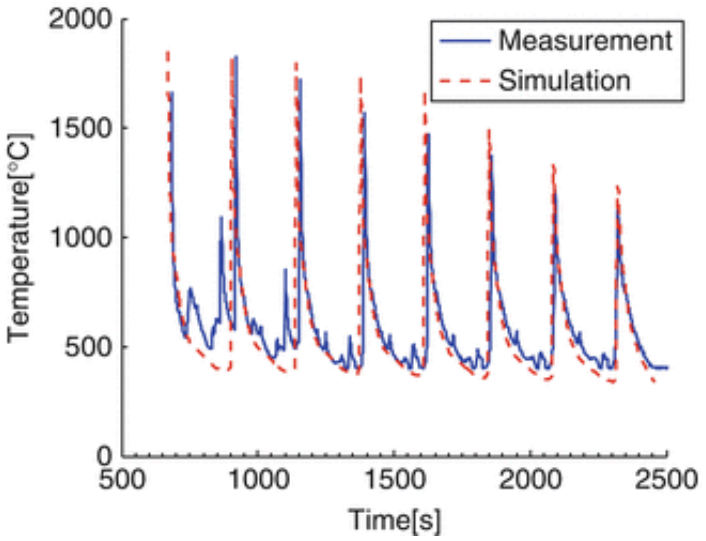

Fig. 9

Measured and computed temperatures during welding

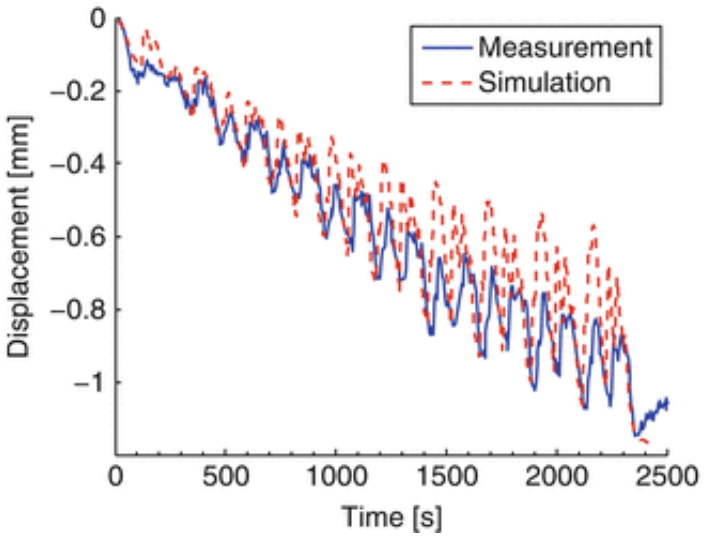

Fig. 10

Measured and computed out-of-plane deformations during welding

Future Development

Two strands have been identified as particularly important for the future development of modeling of SMD. One is the development of constitutive and microstructural models and especially the coupling between these. This is of particular interest in modeling of SMD as a large portion of the material is subjected to multiple heating and cooling cycles. Another area that needs to be assessed is the prediction of the shape of the filler material. As the main focus with SMD is to reduce the amount of scrap, predicting the final shape of the added material is of great importance.

Cross-References

Computational Welding Mechanics

References

1. Lindgren L-E, Runnemalm H, Näsström M (1999) Simulation of multipass welding of a thick plate. Int J Num Meths Eng 44:1301–1316
MATH

2. Lobitz DW, Mc Clure JD, Nickell RE (1977) Residual stresses and distorsions in multi pass welding. In: Numerical modelling of manufacturing processes. Proceedings of the ASME WAM, PVP-PB-25, pp 1–18

3. Lindgren L-E (2001) Finite element modelling of welding. Part 1: increased complexity. J Therm Stress 24:141–192

4. Lindgren L-E (2001) Finite element modelling of welding. Part 2: improved material modeling. J Therm Stress 24:195–231

5. Lindgren L-E (2001) Finite element modelling of welding. Part 3: efficiency and integration. J Therm Stress 24:305–334

6. Chiumenti M, Cervera M, Salmi A, Agelet de Saracibar C, Dialami N, Matsui K (2010) Finite element modeling of multi-pass welding and shaped metal deposition processes. Comput Meth Appl Mech Eng 199:2343–2359
MATH

7. Lundbäck A, Lindgren L-E (2011) Modelling of metal deposition. Finite Elem Anal Des 47:1169–1177

8. Clark D, Bache MR, Whittaker MT (2008) Shaped metal deposition of a nickel alloy for aero engine applications. J Mater Process Technol 203(1–3):439–448

9. Baufeld B, Van der Biest O, Gault R, Ridgway K (2011) Manufacturing Ti–6Al–4V components by shaped metal deposition: microstructure and mechanical properties. In: IOP conference series: materials science and engineering 26, 012001 doi:10.1088/1757-899X/26/1/012001

10. Cervera M, Agelet de Saracibar C, Chiumenti M (2002) COMET – A coupled mechanical and thermal analysis code. Data input manual. Version 5.0. Technical Report IT-308, CIMNE

11. Chiumenti M, Agelet de Saracibar C, Cervera M (2008) On the numerical modelling of the thermo-mechanical contact for metal casting analysis. J Heat Transf 130:1–10

12. Babu B (2008) Physically based model for plasticity and creep of Ti-6Al-4V. Division of Material Mechanics, Luleå University of Technology, Luleå

13. Agelet de Saracibar C, Cervera M, Chiumenti M (1999) On the formulation of coupled thermoplastic problems with phase-change. Int J Plasticity 15:1–34
MATH

14. Hunzinker O, Dye D, Roberts SM, Reed RC (1999) A coupled approach for the prediction of solidification cracking during the welding of superalloys. In: Proceedigs of the conference on numerical analysis of weldability, Graz-Seggau, Austria

15. Lindgren L-E (2007) Computational welding mechanics: thermo-mechanical and microstructural simulations. CRC Press, Boca Raton

16. Cervera M, Agelet de Saracibar C, Chiumenti M (1999) Thermomechanical analysis of industrial solidification processes. Int J Num Meths Eng 46:1575–1591
MATH